

The effect of an active thermal coating on efficiency and emissions from a high speed direct injection diesel engine

Nick Papaioannou, Felix Leach, Martin Davy
Department of Engineering Science, University of Oxford, UK

Robert Gilchrist
Thistle Dubh Ltd., UK

SAE Technical Paper – Author's Accepted Manuscript

Abstract

This study looked into the application of active thermal coatings on the surfaces of the combustion chamber as a method of improving the thermal efficiency of internal combustion engines. The active thermal coating was applied to a production aluminium piston and its performance was compared against a reference aluminium piston on a single-cylinder diesel engine. The two pistons were tested over a wide range of speed/load conditions and the effects of EGR and combustion phasing on engine performance and tailpipe emissions were also investigated. A detailed energy balance approach was employed to study the thermal behaviour of the active thermal coating. In general, improvements in indicated specific fuel consumption were not statistically significant for the coated piston over the whole test matrix. Mean exhaust temperature showed a marginal increase with the coated piston of up to 6 °C. However, the normalised exhaust enthalpy showed a reduction (apart from the higher speed/load conditions when no EGR was applied). Energy transfer to the coolant was reduced by as much as 1.5 percentage points, in agreement with the expected reduction in piston heat transfer, across all operating conditions. Finally, soot emissions were increased with the coated piston, with the biggest differences between the coated and non-coated pistons observed at the lower speed/load conditions.

Introduction

The upcoming 2021 CO₂ emission standards for all new vehicles are posing a significant challenge to automotive manufacturers. With these limits set to be reduced further in the following years, new technologies that increase the thermal efficiency of the internal combustion engine and consequently reduce the tailpipe CO₂ emissions are necessary.

One way of achieving an improvement in thermal efficiency is to reduce the amount of fuel energy that is transferred as heat to the coolant, which currently varies between 30-45 % of the fuel energy depending on operating conditions and engine type [1]. In the past the concept of adiabatic engines have been thoroughly studied where ceramic coatings were employed in the combustion chamber surfaces to reduce the amount of heat transferred to the surroundings [2, 3].

The lower thermal conductivity of ceramic coatings compared to metals, results in higher surface temperatures and consequently, according to Newton's law of cooling, the heat convected to the

combustion chamber surfaces is reduced. Studies have shown that heat conduction between the piston and the cylinder walls significantly contributes to the energy transfer to the coolant. More specifically, depending on the cooling approach, approximately, 30-65 % of the heat flow through the piston crown can be transferred to the cylinder wall via the piston ring pack and the piston skirt and from there to the coolant [4]. Figure 1 shows a typical conversion of fuel energy in an internal combustion engine. Consequently, reducing the heat transferred to the piston by employing ceramic coatings results in an improvement in thermal efficiency as more energy is converted into piston work. However, such coatings apart from their low thermal conductivity also exhibit high heat capacity, which translates to a slower rate of cooling during the intake period and consequently, to a reduction in volumetric efficiency as the intake charge temperature is increased. In addition the consequent increased risk of knock (in a spark ignition engine) would lead to reductions in efficiency.

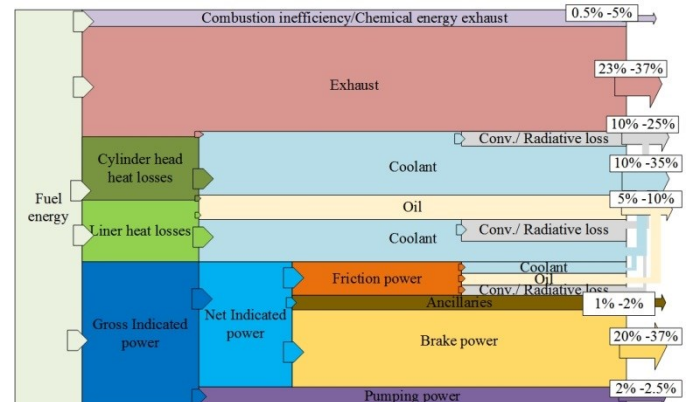


Figure 1: Typical fuel energy breakdown in internal combustion engines. Values are shown as a percentage of fuel energy and are only indicative.

The use of ceramic thermal barrier coatings typically results in increased NO_x emissions due to increased in-cylinder temperatures [5, 6]. However, these higher cylinder temperatures have also been shown to result in higher exhaust temperatures [7, 8] which may be advantageous to the exhaust after-treatment system and as such the NO_x penalty might be offset by improved after-treatment performance particularly during cold-start. In addition the higher

exhaust temperatures would prove beneficial to any exhaust waste heat recovery systems.

In order to remove the negative effects of thermal barrier coatings on the volumetric efficiency of an engine, a combination of low heat capacity and low thermal conductivity must be used. Such a coating was first introduced by Toyota with their silica reinforced porous anodized aluminium (SiRPA) insulation material [7-9]. The thermal properties of this coating allowed for the surface temperature of the piston to be closer to the combustion gas temperature thus reducing heat losses to the piston while at the same time rejecting heat at a higher rate during the exhaust valve opening period thus not impeding volumetric efficiency. The SiRPA coating was reported to give small improvements in thermal efficiency (< 2 %) and exhaust gas temperatures while reducing the energy transferred to the coolant. Similar coatings have been tested by various researchers, where similar improvements, albeit small, were observed [7, 8, 10-12] with some researchers however, reporting a deterioration in fuel consumption when these coating were employed [13].

Significant factors preventing further improvements in efficiency with these coatings are believed to include permeable porosity and the surface roughness of the coating. Increasing a coating's permeability has been shown to reduce thermal efficiency and increase heat losses as fuel/air mixture is trapped in the coating's pores as well as reducing the effective compression ratio [10, 14-16]. Furthermore, Kawaguchi *et al.* [8] found that increased surface roughness results in reduced fuel spray penetration, which has been shown to lead to lower burn rates and reduced efficiency [17], although it must be noted that Kawaguchi *et al.* did not model the combined effects of surface roughness and porosity.

Previous work has not generally considered the changes in emissions resulting from these coatings and have only focused on efficiency gains and reduction in coolant transfer losses. This work aims to provide information on the emissions performance of such coatings. As such two pistons were tested, one reference aluminium piston and one coated with an active thermal coating across its bowl and top-land surfaces. Focus was primarily given on the NO_x-soot characteristics of each piston however their performance was also tested using heat release analysis and a heat balance energy model.

Experimental equipment and methodology

Engine and instrumentation

The engine used in this study was a single-cylinder direct injection diesel engine with the bottom based on a Ricardo Hydra research engine. The engine configuration and its peripherals have been described in detail in previous publications [18, 19]. A split cooling system was employed whereby the cylinder head and cylinder jacket temperatures can be controlled independently. A piston cooling jet was also employed to reduce the operating temperature of the piston. Table 1 presents the details of the test engine.

Table 1: Engine parameters

Parameter	Specification
Bore × Stroke	83mm × 92.4mm
Displacement	500 cm ³

Valves per cylinder	2 intake, 2 exhaust
Fuel system	Common rail
Fuel injector	8-hole solenoid

Crank-angle resolved cylinder pressure data were measured using a piezoelectric Kistler transducer logged with a high-speed data acquisition unit, AVL Indicor, at a resolution of 0.1 CAD. Low frequency channels were logged at 1 Hz using a CADET engine control system by Sierra-CP engineering.

Fuel flow measurements were carried out using both a gravimetric and a coriolis fuel flow meter. The agreement between the two units is within 1 % even at very low flow rates. Emissions measurements were done with a Horiba MEXA-ONE, smoke readings were taken using an AVL-415S smoke meter, and particle number measurements with a Cambustion DMS500. High-accuracy differential thermocouples, employed in past studies [20], were used to measure the small coolant temperature differences across the engine, which provided more accurate input into the energy balance model.

The heat release and mass fraction burn results presented in this work were calculated using the standard package available in AVL Concerto software [21], using the signals from the in-cylinder pressure transducer and that of the shaft encoder. The heat release calculation was carried out between -25 and 135 CAD at a 0.1 CAD resolution

Active thermal coating

The thermal coating used in this work was developed by Keronite Ltd. using a novel plasma electrolytic oxidation (PEO) process. The surface roughness was 4.5 µm R_a on the crown and 3.5 µm R_a in the bowl. A top layer acting as a sealant was also incorporated in order to remove the negative effects of porosity on engine performance. The surface roughness in the bowl of the reference piston was 4 µm R_z. The thermal properties of the active thermal coating can be seen in Figure 2 where they are compared against those of typical materials used for thermal insulation. The thermal coating was applied to the piston crown and bowl areas of a production aluminium piston from the same batch as the reference piston as can be seen in Figure 3.

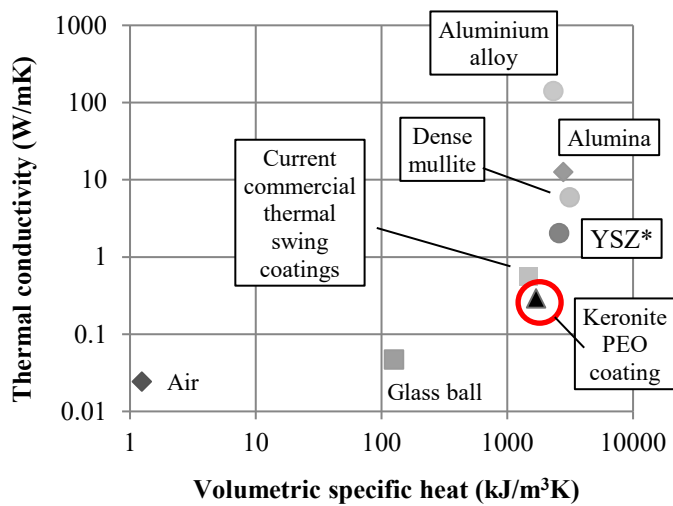


Figure 2: Thermal properties of the active thermal coating.
*Yttria Stabilised Zirconia

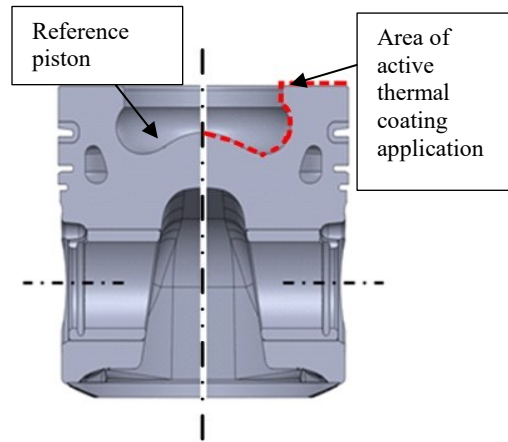


Figure 3: Area of active thermal coating application (not to scale).

Effects of thermal coating porosity on compression ratio

The presence of a piston coating has been shown to have an effect on the resulting CR [10]. In this work, the CR with the two pistons was measured and found to be identical within measurement uncertainty. To validate this further the maximum cylinder pressures (P_{max}) for the two pistons under motoring conditions were also compared. The P_{max} comparison can be seen in Figure 4, where the values presented are averages over a 3 minute log period and then averaged over 10 different test days. The error bars indicate one standard deviation. It is clear that there is a very good agreement between the two pistons in terms of P_{max} which indicates that in this work, the active thermal coating does not have a measurable effect on the compression ratio.

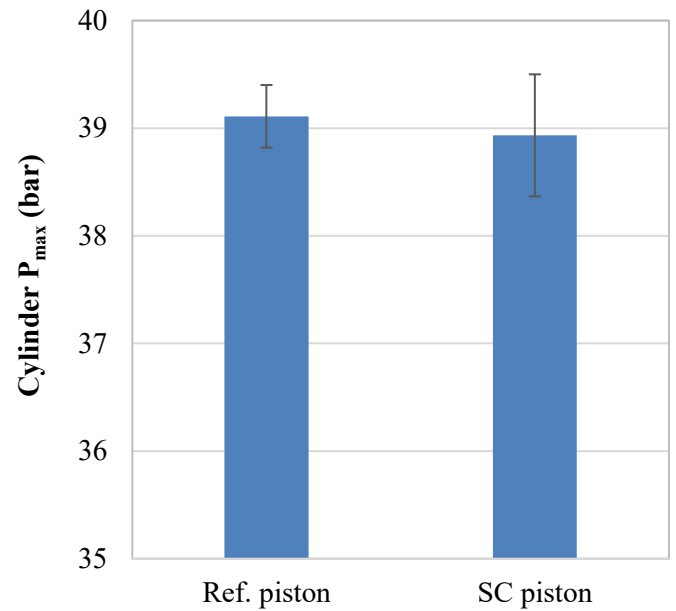


Figure 4: Average P_{max} values for the two pistons tested under motoring conditions. The error bars indicate one standard deviation

Energy balance analysis

The energy balance analysis employs a control volume approach where the energy inputs to the control volume (CV on Figure 5) comprise; the fuel chemical energy, the enthalpy of intake air, the enthalpy of the EGR gases and the heat supplied by the oil sump heaters (note that results are presented as a fraction of this *total* input energy, Q_{in}). The measured or calculated energy out terms from the control volume are: the energy to the oil (Q_{oil}), brake efficiency (Brk. Eff.), energy to the coolant at the cylinder jacket (Q_{cool_jck}) and at the cylinder head (Q_{cool_head}), exhaust enthalpy (Q_{exh}), exhaust chemical energy (Q_{chem}) and a term for extraneous losses (Q_{ext}), which lumps together all of the unaccounted energy terms. All terms are presented as normalised values to the total energy input. The energy balance model is discussed in more detail in previous work [20].

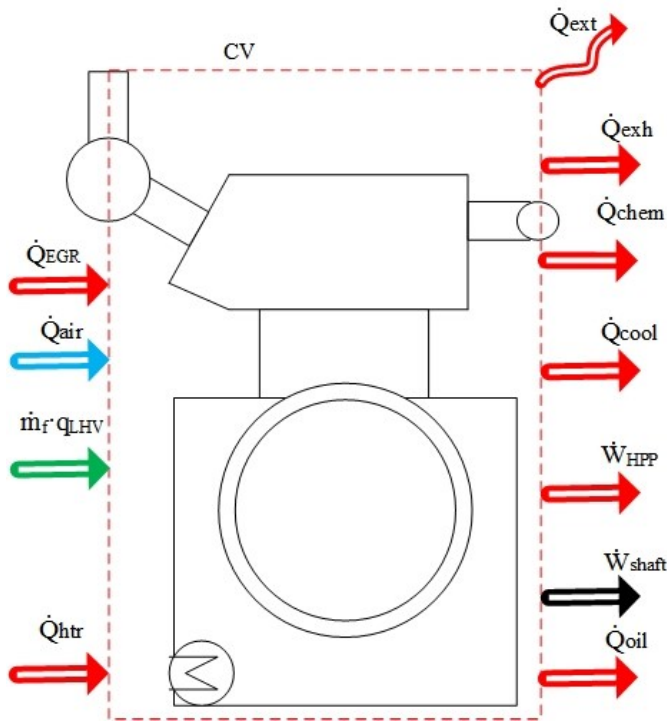


Figure 5: Control volume for the energy balance model used. The inputs to the model are on the left and the outputs on the right [19]

The results presented here are in terms of relative change with respect to the reference aluminium uncoated piston. This means that a positive value indicates an increase and a negative value a decrease for the SC piston relative to the reference piston. Finally all error bars presented for the energy balance results indicate one standard deviation over the three repeats.

Fuel

The tests were run using an EN590 standard diesel containing no oxygenated components. Table 2 shows the properties of the diesel tested.

Table 2: Diesel fuel composition

Cetane Number	53.0
IBP (°C)	171.4
FBP (°C)	355.0
Aromatics (% m/m)	25.1
Sulfur (mg/kg)	6.5
FAME (% v/v)	<0.1

Test procedure

Table 3 shows the operating conditions for the four test cases. The engine was operated at four different speed and load conditions. For each condition a five-point EGR sweep was performed, with the

maximum EGR rate being limited by a smoke reading of approximately 3 FSN. Furthermore, the effects of injection timing were also studied by testing three combustion phasing scenarios for each test point. This was achieved by adjusting the angle of 50 % mass fraction burned (CA50) on the electronic control unit (ECU) which was held constant during testing via a closed-loop controller. The three scenarios included a reference combustion phasing (indicated in Table 3), an advanced combustion phasing (-4 CAD from reference, +CA50) and a retarded combustion phasing (+4 CAD from reference, -CA50). For each combustion phasing setpoint a five-point EGR sweep was performed.

The intake temperature was held constant with the use of an external air heater at the values shown in Table 3. The coolant and oil inlet temperatures were maintained at 90 °C. Each EGR sweep-CA50 combination was repeated three times to provide adequate data for statistical analysis. 1 Hz data was logged for three minutes, and the 0.1 CAD data logged for 300 cycles. Consequently, all error bars presented in this work indicate one standard deviation over that three minute log or 300 cycles. When error bars are not visible, these are small enough to be hidden by the markers in the graphs. Finally it should be noted that all emissions and fuel consumption data have been rescaled by dividing the values by an arbitrary number selected to give peak values around 1 (the same value for every plot) for reasons of commercial confidentiality.

Table 3: Engine operating conditions

Test point	TP 1	TP 2	TP 3	TP 4
Speed (rpm)	1500	1500	2000	2500
nIMEP (bar)	3.8	6.9	12.3	17.7
Rail pressure (MPa)	58	67	116	147
CA50 (deg)	6.5/10.5/14.5	3.1/7.1/11.1	6/10/14	9.3/13.3/17.3
Intake T (°C)	55	40	40	40

Results

Standard injection timing

Figures 6 and 7 show the ISNO_x-soot results for test points (TP) 1 and 3 respectively with standard combustion phasing. Overall, the results show that NO_x-soot trade-off is worsened with the piston employing the temperature swing coating (SC) with the exception of TP1 (similar trends to TP3 case are observed for TP2 and TP4 and are not shown here). Minor differences between pistons in the observed ISNO_x-soot tradeoff at very low levels of NO_x in Figure 6 can be attributed to small differences in the EGR levels of these operating points.

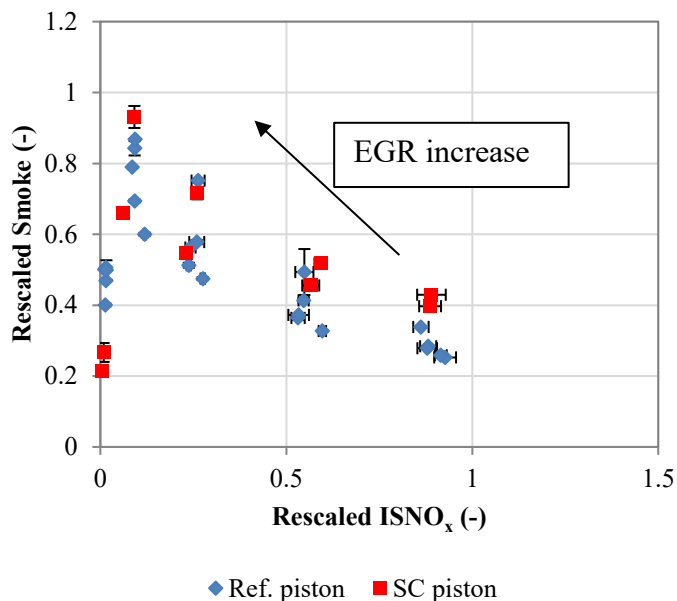


Figure 6: Rescaled ISNO_x-soot results for TP1 with standard injection timing. The error bars indicate $\pm \sigma$

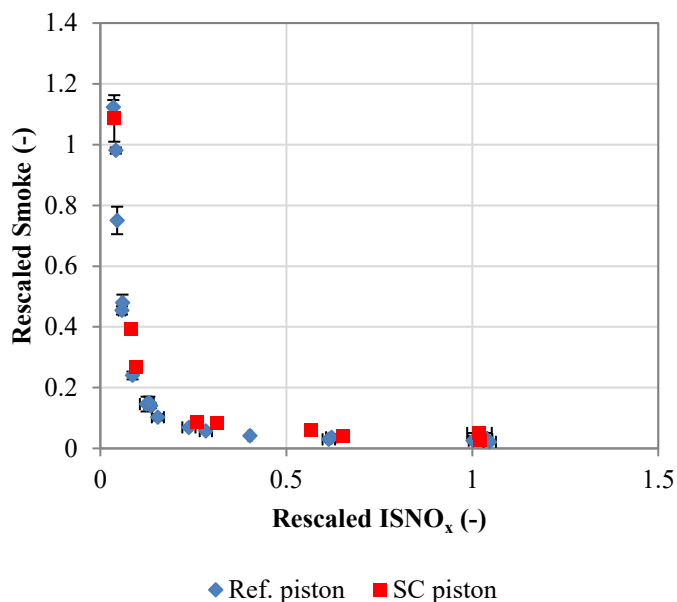


Figure 7: Rescaled ISNO_x-soot results for TP3 with standard injection timing. The error bars indicate $\pm \sigma$

the ISTHC values at TP4. Similarly, no discernible differences exist between the two pistons – and this result was true at all other TPs.

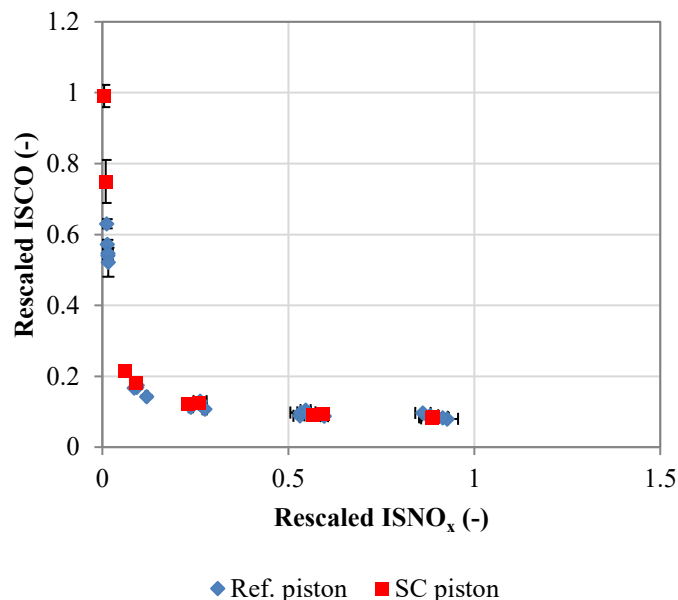


Figure 8: Rescaled ISCO results against rescaled ISNO_x for TP1 conditions for all injection timings. The error bars indicate $\pm \sigma$

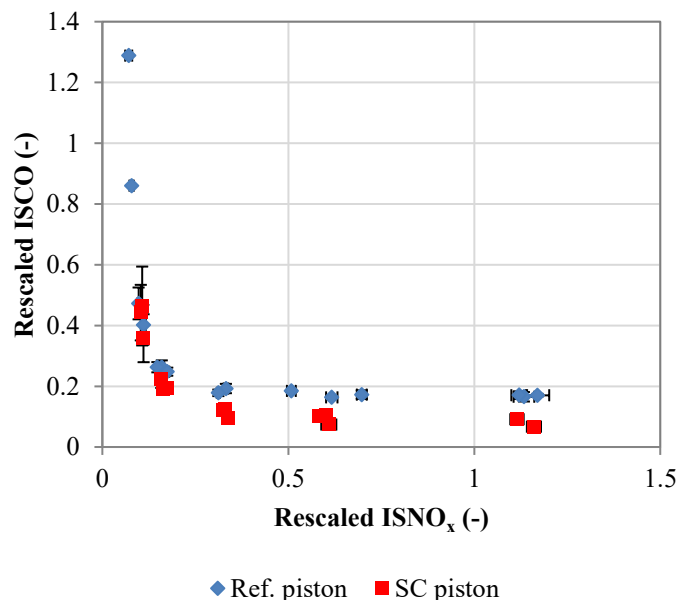


Figure 9: Rescaled ISCO results against rescaled ISNO_x for TP4 conditions for all injection timings. The error bars indicate $\pm \sigma$

Figure 8 and 9 show the ISCO values against the ISNO_x results for TP1 and TP4 conditions respectively. For TP1 no differences are observed between the two pistons with some differences being obvious for the TP4 (the highest speed/load) conditions where ISCO emissions are decreased with the swing coated piston, possibly as a result of higher temperatures promoting $\text{CO} \rightarrow \text{CO}_2$ oxidation with the swing coated piston. It should be noted that it was not always possible to achieve exactly the same maximum EGR rate which explains the more pronounced deviations on the left hand side of the graphs which corresponds to the highest EGR rate. Figure 10 shows

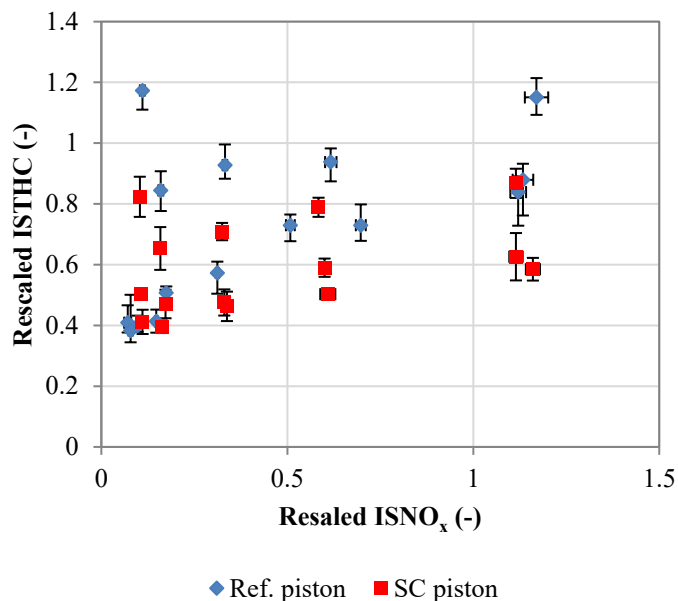


Figure 10: Rescaled ISTHC values against rescaled ISNO_x for TP4 conditions for all injection timings. The error bars indicate $\pm\sigma$

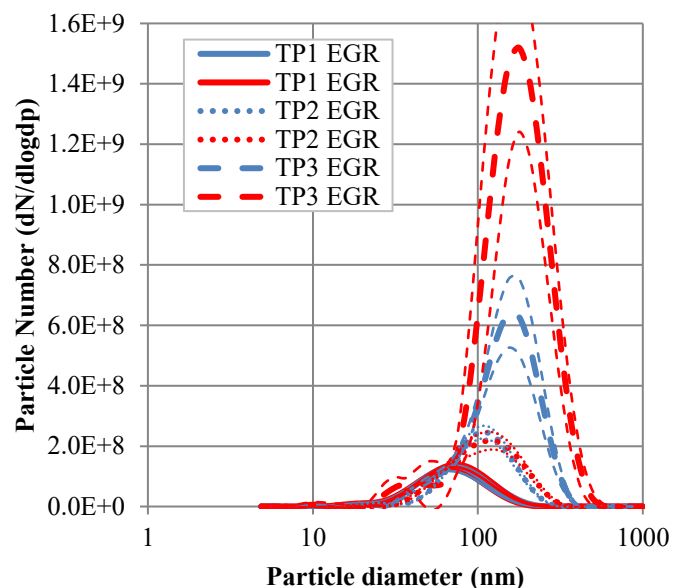


Figure 12: Particle size distributions for TPs 1-3 with EGR. The blue lines are the reference piston and the red lines the SC piston. The narrow bands correspond to $\pm\sigma$

Figures 11 and 12 show the particle size distributions for points with (Fig 11) and without (Fig 12) EGR. For each graph, the blue (dark) lines are the results from the reference piston, and the red lines from the SC piston (readers are referred to the online version of this paper for full-colour). It can be seen that there are only very minor differences in particle size distribution with the SC piston, with most of the points falling within one standard deviation. The differences in Figure 12 at TP3 can be attributed to minor variations in EGR levels.

Figures 13 and 14 show the ISFC values for TP1 and TP4 cases respectively. It is clear that the SC piston does not show any statistically significant benefit over the reference piston and this is true for all conditions tested. A small increase in ISFC with EGR can be seen in Figure 14 consistent with the slower burn rates and reduced oxidation (refer to Figure 9) observed with EGR use.

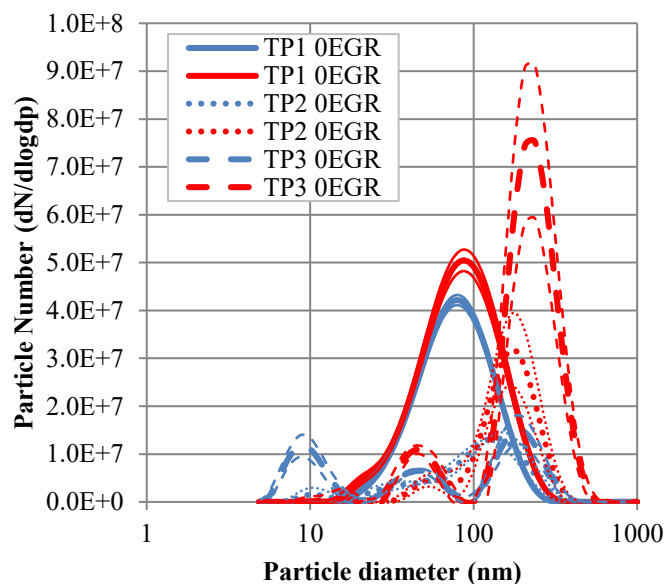


Figure 11: Particle size distributions for TPs 1-3 without EGR. The blue lines are the reference piston and the red lines the SC piston. The narrow bands correspond to $\pm\sigma$

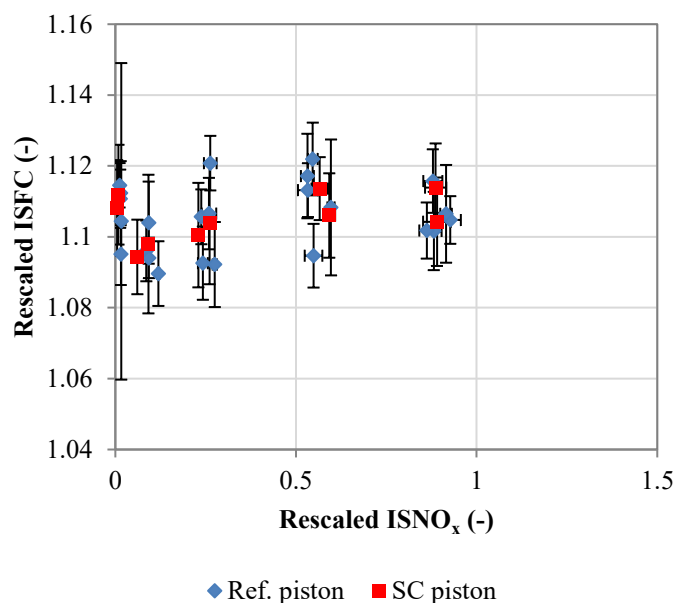


Figure 13: Rescaled ISFC values against rescaled ISNO_x for TP1 with standard injection timing. The error bars indicate $\pm\sigma$

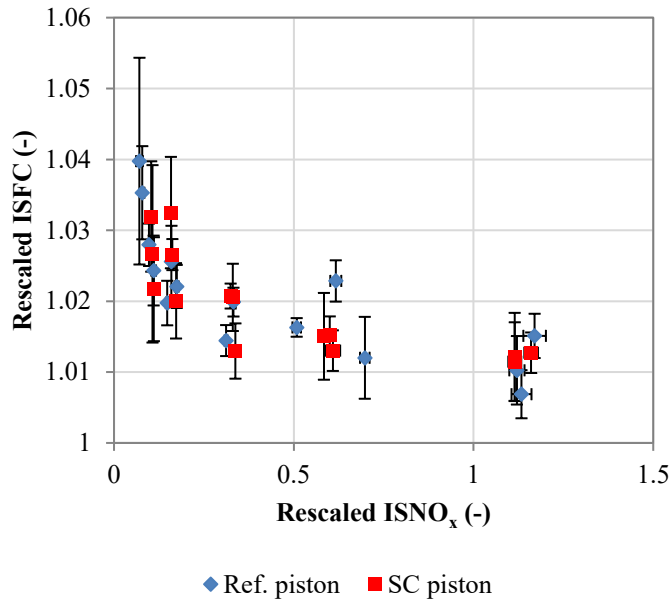


Figure 14: Rescaled ISFC values against rescaled ISNO_x for TP4 with standard injection timing. The error bars indicate $\pm \sigma$

Figure 15 and 16 show the exhaust temperature results for TP1 and TP4 respectively. From the graphs it can be seen that the exhaust temperature is increased with the SC piston for TP1 by $\sim 6^\circ\text{C}$ on average irrespective of EGR rate. However, as the load and speed increases the increased exhaust gas temperature with the SC piston is lost as can be seen in the extreme case of TP4 in Figure 16. This could be due to the reduction in available time for heat transfer as engine speed is increased which is negating the positive effects of the active thermal coating.

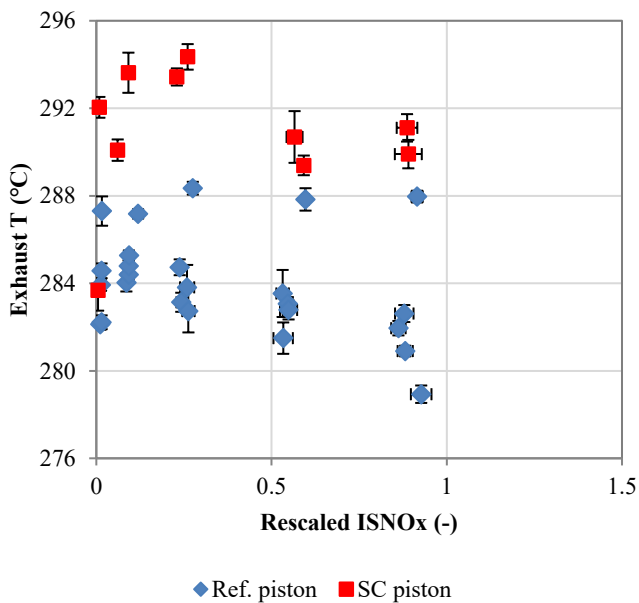


Figure 15: Exhaust temperature against ISNO_x values for TP1 with standard injection timing. The error bars indicate $\pm \sigma$

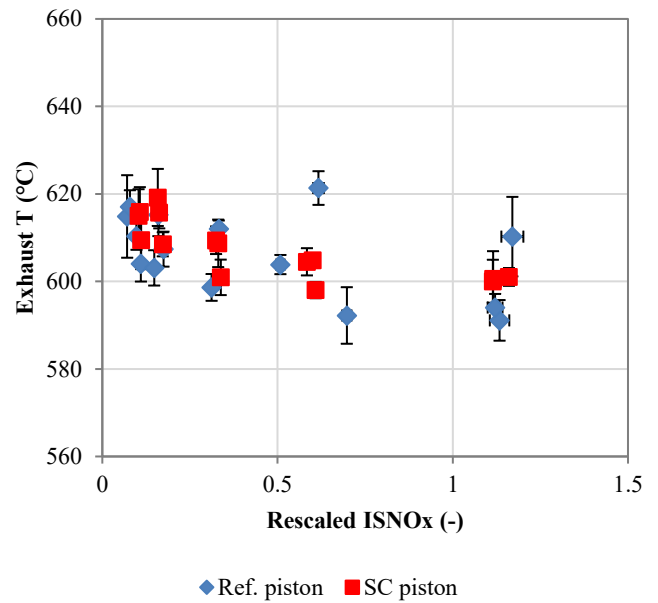


Figure 16: Exhaust temperature against ISNO_x values for TP4 with standard injection timing. The error bars indicate $\pm \sigma$

Energy balance results

Figure 17 shows the energy balance at TP4, 0 % EGR. The results are presented as a percentage of the total input energy. It can be seen that the dominant energy flows are to brake power, the oil and coolant, and to the exhaust. Figures 18 and 19 show the results of the energy balance study in terms of energy change for the two pistons (normalized to the percentage of total input energy for each case), for TP4 conditions, at maximum EGR rate and without EGR. In general, very small differences are observed, across all test points and EGR rates, with the majority of the test points not showing statistically significant differences. However, as a general trend the energy to the coolant was reduced and the exhaust and extraneous enthalpies were increased. When EGR is added (Figure 19) the magnitude of energy change to the coolant and the exhaust is relatively unchanged. Although the differences are relatively minor, as a percentage change the swing coated piston sees about a 10 % reduction in energy to the coolant and a 1 % increase in energy to the exhaust. TP4 is representative of the energy flows at other points.

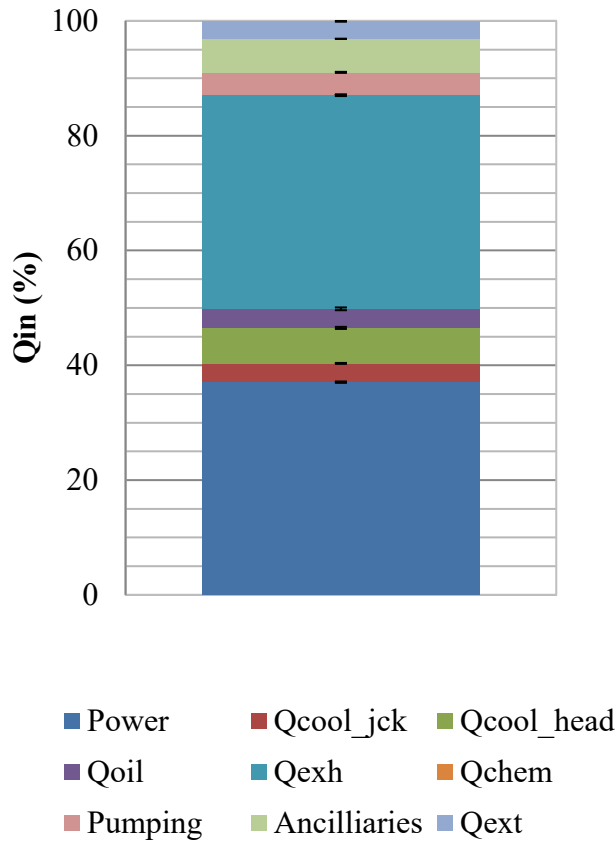


Figure 17: Energy balance results for the reference piston at TP4, 0 % EGR. The error bars indicate $\pm \sigma$

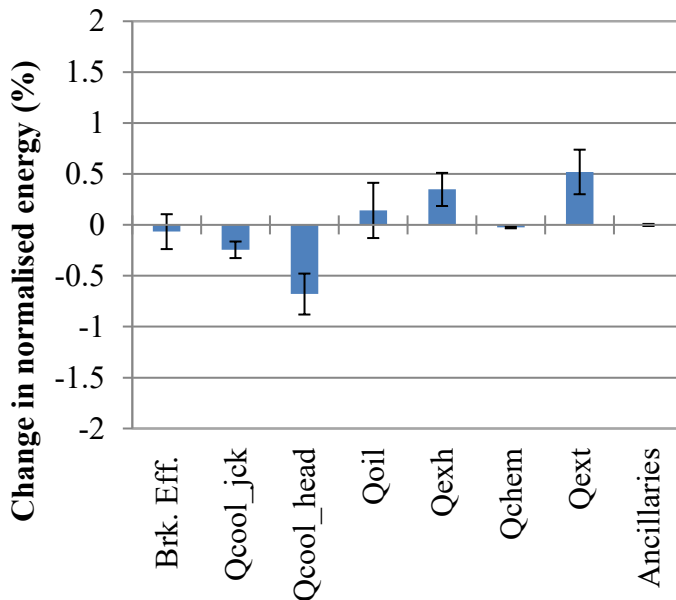


Figure 18: Change in energy transfer terms with respect to the SC piston for TP4 - 0 % EGR rate. The error bars indicate $\pm \sigma$

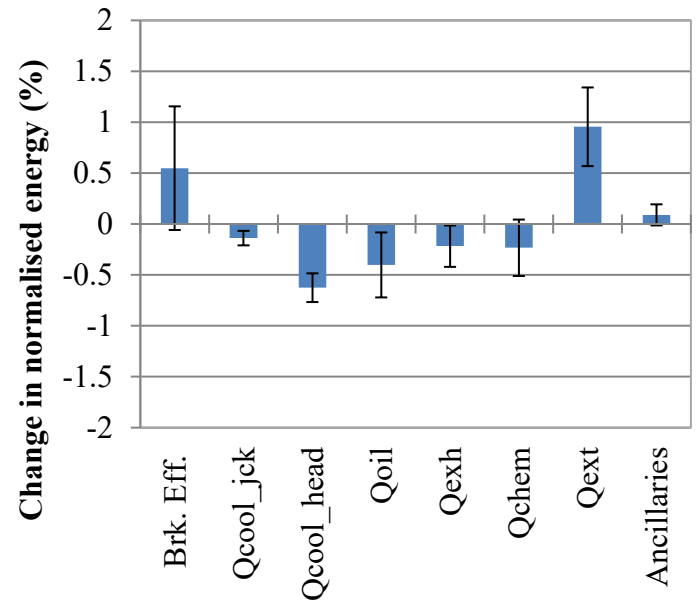


Figure 19: Change in energy transfer terms with respect to the SC piston for TP4 – max EGR rate. The error bars indicate $\pm \sigma$

Effects of injection strategy

In terms of emissions, similar trends to the standard injection timing were observed, that is the NO_x -smoke trade-off was slightly worse with the SC piston independent of injection strategy. Figure 20 shows the smoke-IS NO_x results for TP1 for the different injection strategies. As it can be seen, the SC results in higher smoke values independent of injection strategy, with the highest smoke values resulting from the retarded injection strategy. When speed and load are increased these discrepancies are reduced to the point where no statistically significant differences exist, independent of injection strategy. This can be seen in Figure 21 where the smoke-IS NO_x results for the TP3 are shown.

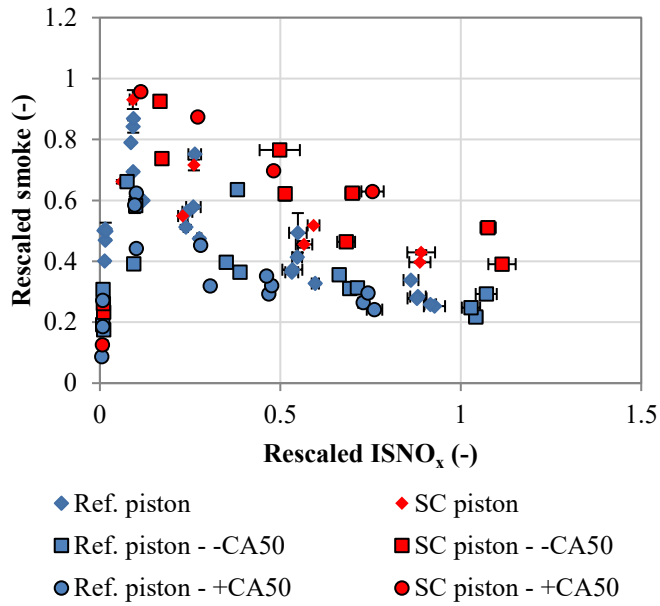


Figure 20: Rescaled smoke against rescaled ISNO_x values for TP1 conditions for all injection strategies. The error bars indicate $\pm \sigma$

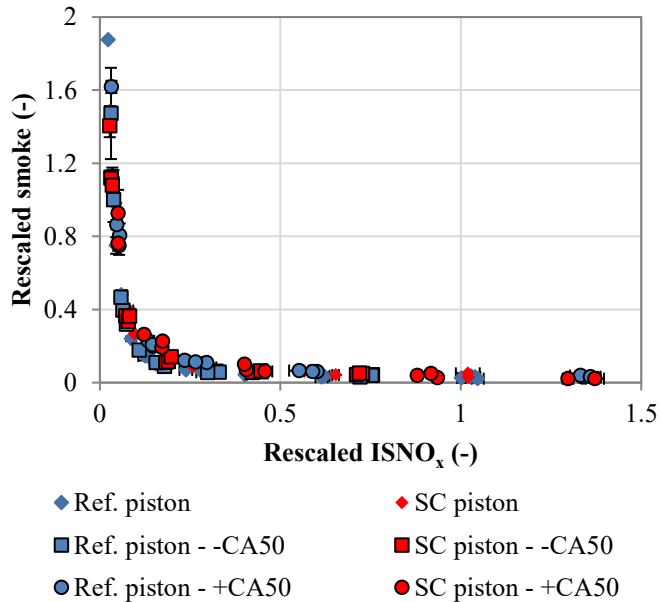


Figure 21: Rescaled smoke against rescaled ISNO_x values for TP3 conditions for all injection strategies. The error bars indicate $\pm \sigma$

Figures 22 and 23 show the ISCO results for TP1 and TP3 conditions. The effect of injection timing on ISCO emissions is insignificant, independent of speed/load conditions. Furthermore, no differences exist between the two pistons under TP1 conditions. For the TP3 case ISCO is reduced by the swing coating (Figure 23) independent of injection strategy. This decrease is of the order ~ 0.2 g/kWh. ISTHC does not show significant differences between injection strategies as well as between pistons at TP1 (Figures 24), however a significant reduction in ISTHC is observed at TP3 (Figure 25), which correlates with increased oxidation observed in Figure 23

with the SC piston. It is possible that at this higher speed/load condition the swing coating leads to preferential conditions for oxidation (higher temperatures) in-cylinder.

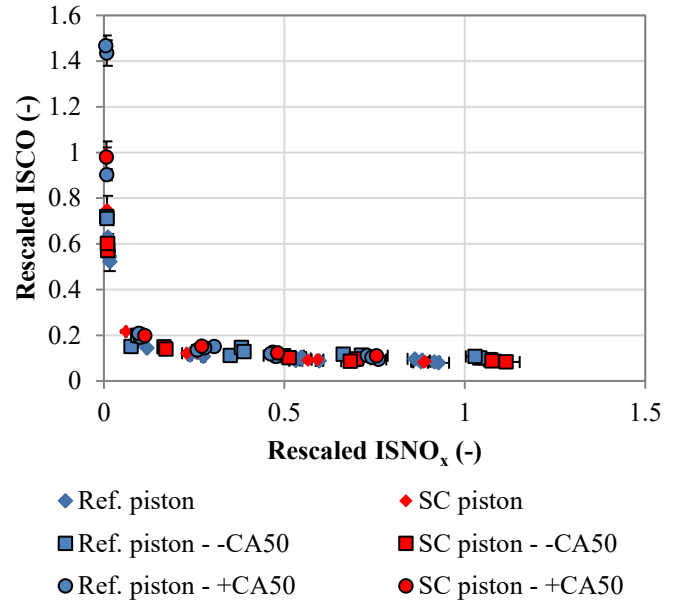


Figure 22: Rescaled ISCO results against rescaled ISNO_x for TP1 conditions for all injection timings. The error bars indicate $\pm \sigma$

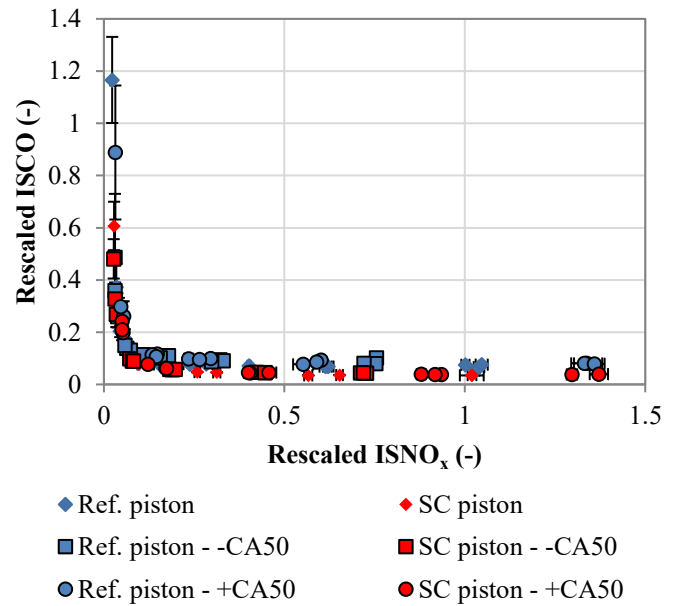


Figure 23: Rescaled ISCO results against rescaled ISNO_x for TP3 conditions for all injection timings. The error bars indicate $\pm \sigma$

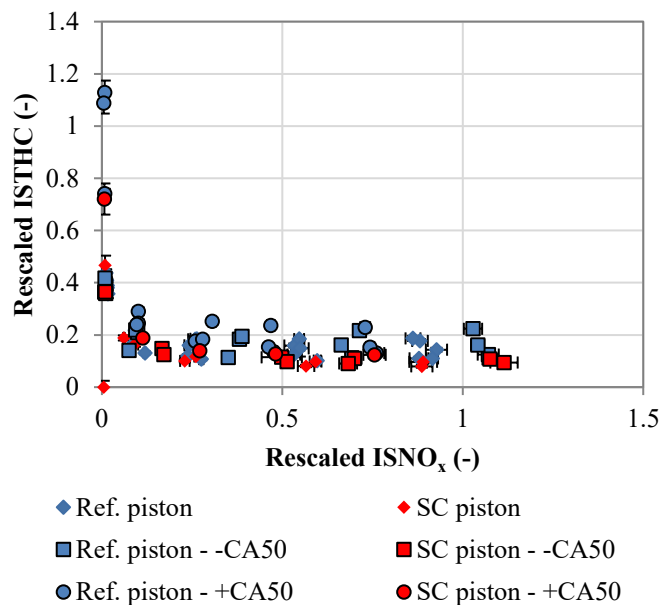


Figure 24: Rescaled ISTHC values against rescaled ISNO_x for TP1 conditions for all injection timings. The error bars indicate $\pm \sigma$

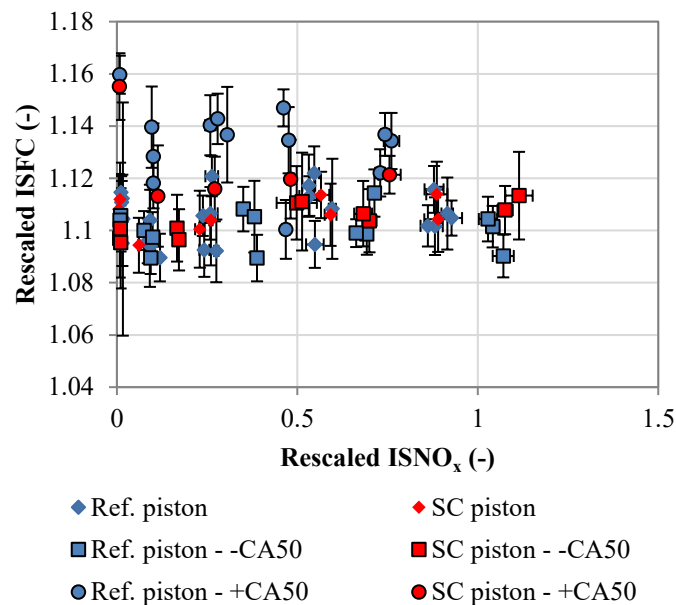


Figure 26: Rescaled ISFC results against rescaled ISNO_x for TP1 conditions for all injection timings. The error bars indicate $\pm \sigma$

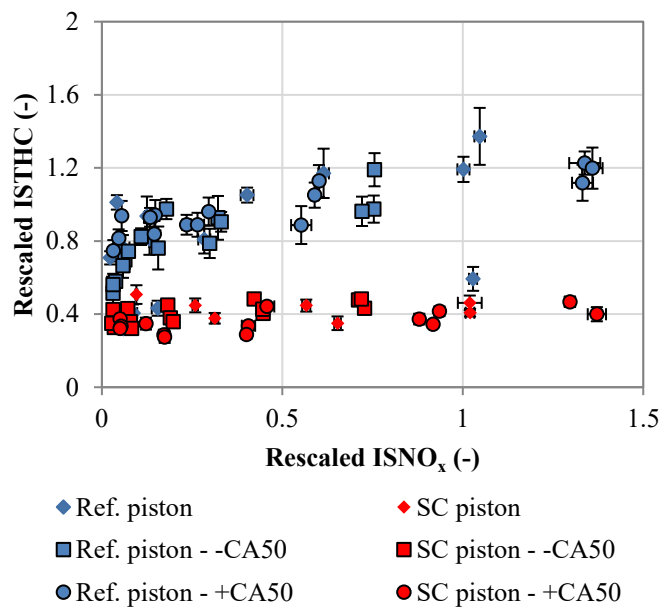


Figure 25: Rescaled ISTHC values against rescaled ISNO_x for TP3 conditions for all injection timings. The error bars indicate $\pm \sigma$

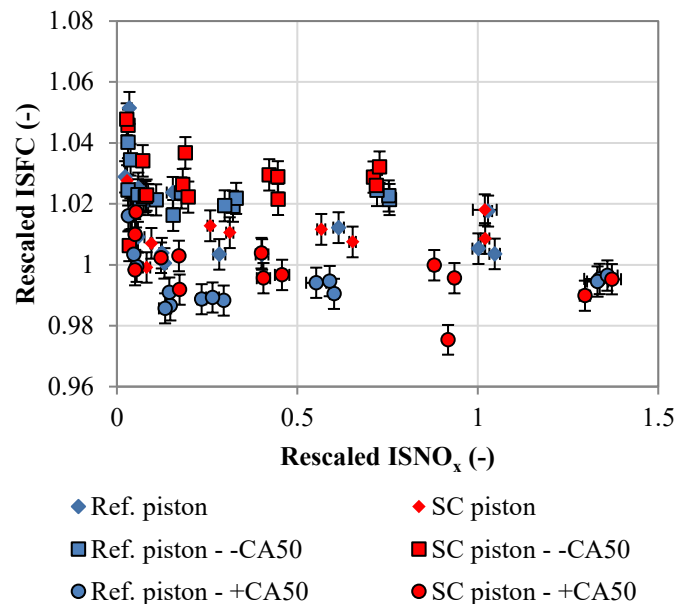


Figure 27: Rescaled ISFC results against rescaled ISNO_x for TP3 conditions for all injection timings. The error bars indicate $\pm \sigma$

In general, advancing the injection timing resulted in an improvement in ISFC, independent of the piston used, as would be expected. Under lower speed/load no statistically significant improvement was observed. Equally, differences between the two pistons were not observed in terms of ISFC, irrespective of injection timing, with the exception of TP1 where the swing coating, under the advanced combustion phasing, (Ref. piston- +CA50) did result in decreased ISFC of ~2 %. This can be seen in Figure 26. Figure 27 shows the ISFC results for the TP3 case across all injection timings.

Exhaust temperature presents similar trends to Figure 15 and 16 independent of injection strategy. More specifically, the SC piston results in an increase in exhaust temperature of ~7 °C depending on test conditions, with this difference being statistically insignificant as load/speed increases. This can be seen in Figure 28 where the exhaust temperature for TP1 is shown.

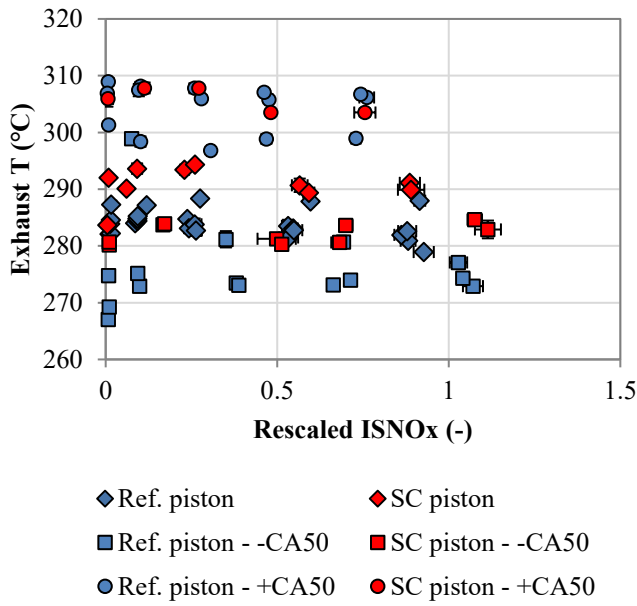


Figure 28: Exhaust temperature against ISNO_x values for TP1 conditions for the different injection strategies tested. The error bars indicate $\pm \sigma$

In terms of energy transfer rates, similar trends to the reference injection timing were observed. That is, when the differences were statistically significant, the energy transfer to the coolant was decreased for the SC piston. However, for these tests the exhaust enthalpy change was statistically insignificant across all test points with the exception of TP4 where the exhaust enthalpy reduced for the SC piston for the retarded injection timing independent of EGR rate. Cumulatively, however, the decreases in enthalpy observed with the SC piston are transferred to the extraneous enthalpy. This was due to a small increase in the input energy to the system for the SC piston (the changes in absolute values of exhaust enthalpy were statistically insignificant). The energy transfer rate changes for TP4 - 0 % EGR rate and advanced injection timing are presented Figure 29.

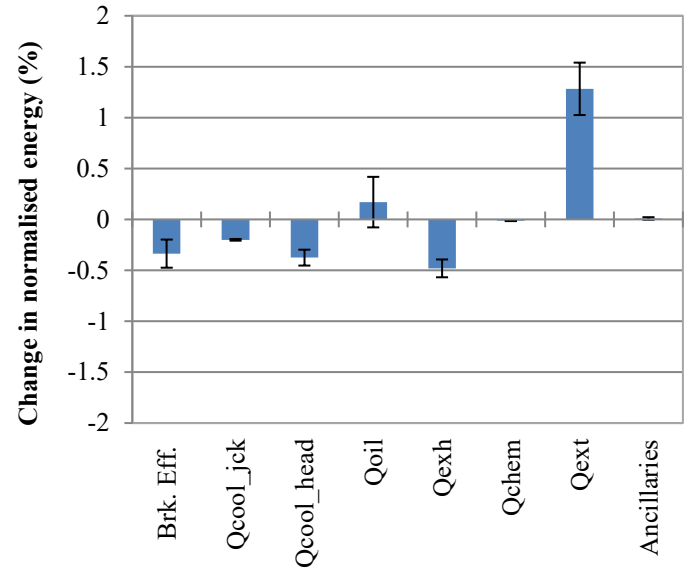


Figure 29: Change in energy transfer terms for TP4-0 % EGR rate and retarded injection timing. The error bars indicate $\pm \sigma$

Heat release analysis results

Figures 30 and 31 show the cumulative heat release and rate of heat release results for all test points under reference injection timings and 0 % EGR rate. Across the conditions tested no clear differences are observed. This indicates that no discernible effects take place in terms of combustion delay, progression and duration from the active thermal coating. It is recalled that the centre of combustion was fixed during testing via a close loop controller. Equally, no statistically significant differences were observed for the two injection strategies across all test conditions and are thus not presented here.

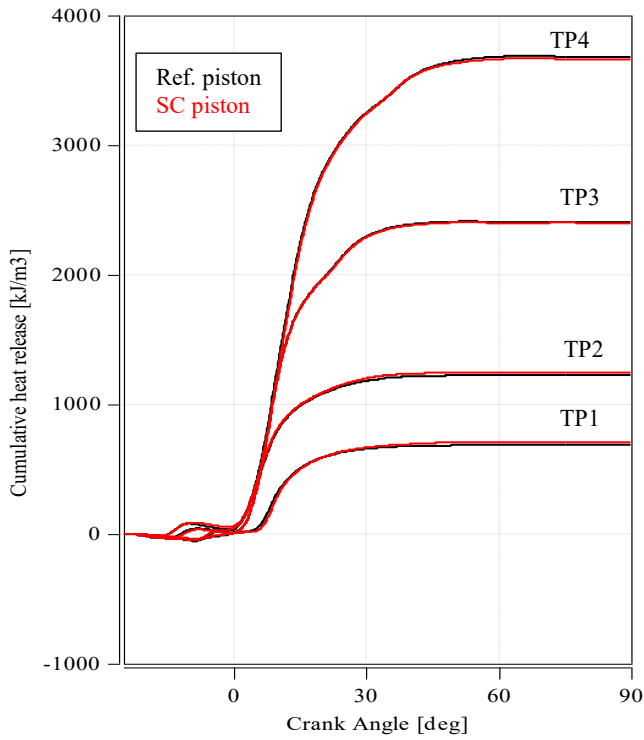


Figure 30: Cumulative heat release results for all test points at reference injection timings and 0 % EGR rate. The black line represents the reference piston and the red line the SC piston

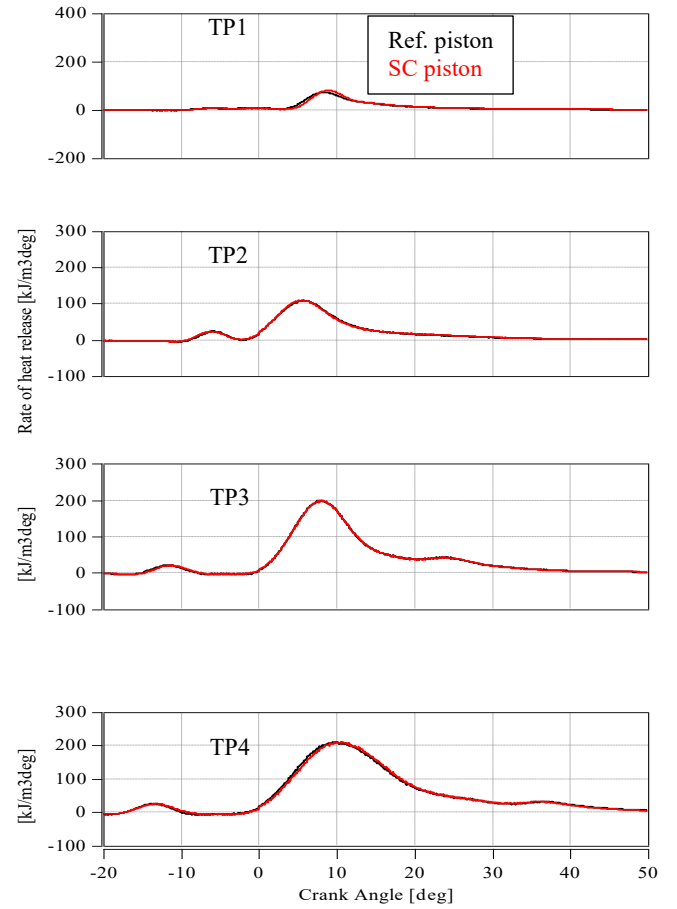


Figure 31: Rate of heat release for all test points at reference injection timing and 0 % EGR rate. The black line represents the reference piston and the red line the SC piston

Discussion

Within the literature swing coated insulations have been promoted as a means of improving engine efficiency and increasing exhaust temperatures by reducing heat transfer to the coolant. However, the gains in efficiencies with the coating employed in this current work are so small as to be essentially immeasurable. This partly agrees with the published studies where the improvements in efficiency were in the order of 0.4 % [10] although in the work presented here it was shown that such differences might be masked by measurement uncertainties when these are taken into consideration.

It has been shown that the surface roughness [8] and the permeable porosity [10, 13] can have an adverse effect on the expected gains in efficiency. An increase in surface roughness has the potential to increase heat transfer losses due to a higher surface area [22]. At the same time increased surface roughness can affect the fuel/air mixing as it inhibits spray penetration at the centre of bowl thus leading to a poorer fuel/air mixing [19, 23]. Consequently this can result in longer burn duration and increased smoke emissions due to locally higher equivalence ratios.

The reduced energy transfer to the coolant with the SC piston, independent of injection strategy and EGR rates, indicates that the surface roughness of the tested coating did not have a detrimental effect on heat transfer losses, or at least that surface roughness does not dominate the heat transfer process on the piston in this case.

On the other hand, the increased smoke emissions observed for the SC piston agree with the thesis of poorer fuel/air mixing at the centre of the bowl. Equally however, the expected higher surface temperatures with the SC piston could also result in increased pyrolysis of the fuel rich spray core thus also increase soot formation rates while suppressing oxidation rates due to the locally rich fuel/air ratio [24]. Looking at the ISCO and ISTHC results helps in understanding this further.

Poor fuel/air mixing can result in incomplete combustion which tends to increase CO and THC – these emissions can also increase with excessive mixing caused by high swirl rates that increase heat transfer losses and can lead to flame extinctions [20]. However, the results show that ISCO emissions are increased for the reference piston under TP3 conditions with the ISTHC results being essentially the same. No appreciable differences are observed for the TP1 case. This implies that given the conditions for TP4 case are the least favorable for mixing (i.e. higher fuel quantity and less time for mixing due to higher engine speed) the swing coating used does not seem to have an effect on fuel/air mixing and that the increased smoke emissions observed with the SC piston might be due to higher piston surface temperatures (although these were not measured in this work).

Published research is showing mixed results in terms of the effect of permeable porosity on efficiency. The porosity of the ceramic coatings has been shown to lead to increased heat transfer losses (increased surface area) as well as result in fuel absorption in the pores, thus resulting in longer combustion duration and reduced efficiency [13, 15]. Another way of impacting efficiency is the reduction in compression ratio due to the porosity of the coating. On the other hand, a recently published work by Somhorst *et al.*, [10] has shown that a high porosity coating presented the biggest improvement in efficiency when compared against a series of varying porosity coatings.

For the work presented here it has already been shown that the ceramic coating did not have any effect on the resulting CR. Equally, as observed by the heat release analysis results, the combustion duration was essentially the same between the two pistons independent of EGR rate and injection timing. Finally, no increase in CO and THC emissions was observed with the SC piston, both indicators of poor fuel/air mixing. All of the above would indicate that the coating did not have an effect on thermal efficiency.

In terms of exhaust temperature, marginal increases were also observed with the SC piston with the biggest differences observed for the TP1 case (~7 °C). This translates into an increase in exhaust enthalpy of ~0.5 %, however considering the inherent errors associated with temperature measurement in internal combustion engines, the authors expect these gains to be underestimated [25].

The contradictory findings in the literature along with the minimal differences presented in this work indicate that although active thermal coatings may be a promising solution to increased thermal efficiencies, their application is not straightforward. Parameters like squish and swirl flows might be inhibiting any expected gains by increasing heat transfer losses [20]. Equally, running these coatings at higher piston temperatures, by disabling the oil cooling jet, might prove beneficial as the piston temperatures will be increased further thus reducing heat transfer losses.

Conclusions

In this work the effect of an active thermal coating on a high-speed direct injection diesel engine was investigated. The piston with the thermal coating (SC piston) was compared against a reference aluminium piston over four engine test points and a range of EGR rates and three injection strategies. Emissions, heat release and energy balance results showed the following:

- No change in compression ratio was observed with the SC piston, in contradiction to work in the literature which showed that porosity reduced the compression ratio.
- Approximately 10 % less energy was transferred to the coolant with the SC piston compared to the reference piston.
- No statistically significant improvements in terms of fuel consumption were observed with the SC piston.
- An exhaust temperature increase of ~7 °C with the SC piston was observed under low load/speed conditions. No such gains were observed under high speed/load.
- Smoke emissions were increased with the SC piston for the same NO_x values.
- No notable differences in combustion performance were observed with the SC piston.

This work has shown that swing coatings do have an impact on energy flows within a modern diesel engine, notably with less heat being transferred to the coolant as would be expected. However, these seeming advantages are not yet being seen in improvements in emissions or ISFC. Further research is needed to understand the reasons behind this and exploit these expected improvements.

References

1. Heywood, J.B., *Internal Combustion Engine Fundamentals*. 1988: MacGraw-Hill
2. Kamo, R., *Adiabatic diesel-engine technology in future transportation*. Energy, 1987. **12**(10): p. 1073-1080.
3. Osawa, K., Kamo, R., and Valdmanis, E., "Performance of Thin Thermal Barrier Coating on Small Aluminum Block Diesel Engine," SAE Technical Paper 910461, 1991, <https://doi.org/10.4271/910461>.
4. Mahle, *Pistons and engine testing*. 2 ed. ATZ/MTZ-Fachbuch. 2016: Springer Vieweg.
5. Alkidas, A. C., and R. M. Cole. "The Distribution of Heat Rejection from a Single—Cylinder Divided—Chamber Diesel Engine." *SAE Transactions* 90 (1981): 2936-948. <http://www.jstor.org/stable/44643997>.
6. Jaichandar, S. and Tamilporai, P., "Low Heat Rejection Engines – An Overview," SAE Technical Paper 2003-01-0405, 2003, <https://doi.org/10.4271/2003-01-0405>.
7. Wakisaka, Y., Inayoshi, M., Fukui, K., Kosaka, H. et al., "Reduction of Heat Loss and Improvement of Thermal Efficiency by Application of "Temperature Swing" Insulation to Direct-Injection Diesel Engines," *SAE Int. J. Engines* 9(3):1449-1459, 2016, <https://doi.org/10.4271/2016-01-0661>.
8. Kawaguchi, A., Iguma, H., Yamashita, H., Takada, N. et al., "Thermo-Swing Wall Insulation Technology; - A Novel Heat Loss Reduction Approach on Engine Combustion Chamber -," SAE Technical Paper 2016-01-2333, 2016, <https://doi.org/10.4271/2016-01-2333>.
9. Kosaka, H., Wakisaka, Y., Nomura, Y., Hotta, Y. et al., "Concept of "Temperature Swing Heat Insulation" in Combustion Chamber Walls, and Appropriate Thermo-

- Physical Properties for Heat Insulation Coat," *SAE Int. J. Engines* 6(1):142-149, 2013, <https://doi.org/10.4271/2013-01-0274>.
10. Somhorst, J., Uczak De Goes, W., Oevermann, M., and Bovo, M., "Experimental Evaluation of Novel Thermal Barrier Coatings in a Single Cylinder Light Duty Diesel Engine," SAE Technical Paper 2019-24-0062, 2019.
 11. Andrie, M., Kokjohn, S., Paliwal, S., Kamo, L. et al., "Low Heat Capacitance Thermal Barrier Coatings for Internal Combustion Engines," SAE Technical Paper 2019-01-0228, 2019, <https://doi.org/10.4271/2019-01-0228>.
 12. Caputo, S., Millo, F., Cifali, G., and Pesce, F., "Numerical Investigation on the Effects of Different Thermal Insulation Strategies for a Passenger Car Diesel Engine," *SAE Int. J. Engines* 10(4):2154-2165, 2017, <https://doi.org/10.4271/2017-24-0021>.
 13. Thibblin, A., & Olofsson, U. (2019). A study of suspension plasma-sprayed insulated pistons evaluated in a heavy-duty diesel engine. *International Journal of Engine Research*. <https://doi.org/10.1177/1468087419879530>
 14. Beardsley, M., Happoldt, P., Kelley, K., Rejda, E. et al., "Thermal Barrier Coatings For Low Emission, High Efficiency Diesel Engine Applications," SAE Technical Paper 1999-01-2255, 1999, <https://doi.org/10.4271/1999-01-2255>.
 15. Andruskiewicz, Peter, Paul Najt, Russell Durrett, and Raul Payri. "Assessing the Capability of Conventional In-Cylinder Insulation Materials in Achieving Temperature Swing Engine Performance Benefits." *International Journal of Engine Research* 19, no. 6 (August 2018): 599–612. doi:[10.1177/1468087417729254](https://doi.org/10.1177/1468087417729254).
 16. Uchida, N. and Osada, H., "A New Piston Insulation Concept for Heavy-Duty Diesel Engines to Reduce Heat Loss from the Wall," *SAE Int. J. Engines* 10(5):2565-2574, 2017, <https://doi.org/10.4271/2017-24-0161>.
 17. Leach, F., R. Ismail, and M. Davy, *Engine-out emissions from a modern high speed diesel engine – The importance of Nozzle Tip Protrusion*. Applied Energy, 2018. **226**: p. 340-352, <https://doi.org/10.1016/j.apenergy.2018.05.117>
 18. Papaioannou, N., Leach, F., and Davy, M., "Thermal Analysis of Steel and Aluminium Pistons for an HSDI Diesel Engine," SAE Technical Paper 2019-01-0546, 2019, <https://doi.org/10.4271/2019-01-0546>.
 19. Leach, F., Ismail, R., Davy, M., Weall, A. et al., "Comparing the Effect of Fuel/Air Interactions in a Modern High-Speed Light-Duty Diesel Engine," SAE Technical Paper 2017-24-0075, 2017, <https://doi.org/10.4271/2017-24-0075>.
 20. Papaioannou, N., Leach, F. C., Davy, M. H., Weall, A., & Cooper, B. (2019). Evaluation of exhaust gas recirculation techniques on a high-speed direct injection diesel engine using first law analysis. *Proceedings of the Institution of Mechanical Engineers, Part D: Journal of Automobile Engineering*, 233(3), 710–726. <https://doi.org/10.1177/0954407017749110>
 21. AVL CONCERTO, in *Application Notes*. 2015.
 22. Celik, N., *Effects of the surface roughness on heat transfer of perpendicularly impinging co-axial jet*. Heat and Mass Transfer, 2011. **47**(10): p. 1209-1217.
 23. Leach, F., et al., *The effect of a stepped lip piston design on performance and emissions from a high-speed diesel engine*. Applied Energy, 2018. **215**: p. 679-689, <https://doi.org/10.1016/j.apenergy.2018.02.076>
 24. Ladommatos, N., Xiao, Z., & Zhao, H. (2005). The effect of piston bowl temperature on diesel exhaust emissions. *Proceedings of the Institution of Mechanical Engineers, Part D: Journal of Automobile Engineering*, 219(3), 371–388. <https://doi.org/10.1243/095440705X6550>
 25. Papaioannou, N., Leach, F., and Davy, M., "Effect of Thermocouple Size on the Measurement of Exhaust Gas Temperature in Internal Combustion Engines," SAE Technical Paper 2018-01-1765, 2018, <https://doi.org/10.4271/2018-01-1765>.

Contact Information

Felix Leach
Department of Engineering Science,
University of Oxford,
Parks Rd,
Oxford,
OX1 3PJ,
UK
Email: felix.leach@eng.ox.ac.uk

Acknowledgments

The authors would like to thank the Jaguar Land Rover Limited and University of Oxford John Fell fund for financial support. Keronite International Ltd. are thanked for spray coating the piston. The authors would also like to thank the Dept. of Engineering Science technicians and maintenance teams for facilities support. Jack Spivey is thanked for data analysis support.

Definitions/Abbreviations

CAD	Crank angle degrees
CA50	Point of 50 % mass fraction burned.
CR	Compression ratio
CV	Control volume
EGR	Exhaust gas recirculation
FAME	Fatty Acid Methyl Ester
IMEP	Indicated mean effective pressure
ISFC	Indicated specific fuel consumption
ISCO	Indicated specific carbon monoxide
ISTHC	Indicated specific total hydrocarbons
PEO	Plasma electrolytic oxidation
SC	Swing coated
TP	Test point

